Exactly Solvable Topological Phase Transition in a Quantum Dimer Model

Laura Shou,[1] Jeet Shah,[1, 2] Matthew Lerner-Brecher,[3] Amol Aggarwal,[4] Alexei Borodin,[3] and Victor Galitski[1]

[1]*Joint Quantum Institute, Department of Physics, University of Maryland, College Park, MD 20742, USA*
[2]*Joint Center for Quantum Information and Computer Science,*
NIST/University of Maryland, College Park, MD 20742, USA
[3]*Department of Mathematics, Massachusetts Institute of Technology, Cambridge, MA 02139, USA*
[4]*Department of Mathematics, Stanford University, Stanford, CA 94305, USA*

We introduce a family of generalized Rokhsar-Kivelson (RK) Hamiltonians, which are reverse-engineered to have an arbitrary edge-weighted superposition of dimer coverings as their exact ground state at the RK point. We then focus on a quantum dimer model on the triangular lattice, with doubly-periodic edge weights. For simplicity we consider a 2×1 periodic model in which all weights are set to one except for a tunable horizontal edge weight labeled α. We analytically show that the model exhibits a continuous quantum phase transition at $\alpha = 3$, changing from a topological $\mathbb{Z}_2$ quantum spin liquid ($\alpha < 3$) to a columnar ordered state ($\alpha > 3$). The dimer-dimer correlator decays exponentially on both sides of the transition with the correlation length $\xi \propto 1/|\alpha - 3|$ and as a power-law at criticality. The vison correlator exhibits an exponential decay in the spin liquid phase, but becomes a constant in the ordered phase. We explain the constant vison correlator in terms of loops statistics of the double-dimer model. Using finite-size scaling of the vison correlator, we extract critical exponents consistent with the 2D Ising universality class.

Introduction— Quantum spin and quantum dimer models [1–7] provide complementary descriptions of strongly correlated phases of matter. In many settings there is an explicit dictionary between the two languages [8–11], with spin-singlet coverings mapped to hardcore dimers on an auxiliary lattice. Within this framework one encounters a rich landscape of phases, ranging from ordered states to a zoo of quantum spin liquids [8, 12, 13]. The latter have been an active topic of research since Anderson's proposal of a resonating valence-bond state in the context of high-T_c cuprates [14], and were later placed in a broader theoretical setting by Kitaev, Wen, and others, linking quantum spin liquids to topics as diverse as frustrated magnetism, emergent gauge theories, and topological quantum error-correcting codes [15–24]. Moreover, quantum dimer models can be realized experimentally using platforms such as Rydberg atom arrays [25–29].

Despite this broad scope, theoretical progress remains hampered by the scarcity of rigorous tools for analyzing these inherently strongly-correlated models. A notable exception is the construction by Rokhsar and Kivelson (RK) [1], which reverse-engineers a local quantum dimer Hamiltonian whose ground state at the RK point is a uniform superposition of dimer coverings, known as the RK wavefunction. At such points, equal-time correlators of diagonal operators reduce to those of a corresponding classical dimer model, allowing one to import powerful tools of classical statistical mechanics and integrable probability, including Kasteleyn's Pfaffian technique on planar graphs [30–33] and its subsequent developments. In this work we generalize the RK construction to produce local Hamiltonians whose ground states realize *arbitrary* edge-weighted superpositions of dimer coverings on arbitrary graphs, where a standard RK Hamiltonian can be defined. This opens the door to exactly solvable models for a much wider class of spin liquids and ordered phases, as well as controlled examples of transitions between them. Furthermore, our Hamiltonian construction implies that a vast

number of results derived for classical edge-weighted dimer models [34–46] are now applicable to a corresponding edge-weighted quantum dimer model. For example, the frozen corners and multiple so-called "smooth" or "gaseous" regions seen in a 2×2 periodic Aztec diamond will also be present in the corresponding quantum dimer model using our construction. We focus here on an analytically tractable quantum dimer model on the triangular lattice that exhibits a continuous quantum phase transition between a topological $\mathbb{Z}_2$ spin liquid and a symmetry-broken ordered state (Fig. 1).

Review of the RK Hamiltonian— The quantum dimer Hilbert space is the span of the orthonormal basis $\{|\mathcal{C}\rangle\}$, where $\mathcal{C}$ denotes a dimer configuration. The RK Hamiltonian [1], written on the square lattice, is

$$H = -J \sum_{\Box} [|\,\text{⦚⦚}\,\rangle \langle\,\text{⊟}\,| + \text{h.c.}]$$
$$+ V \sum_{\Box} [|\,\text{⦚⦚}\,\rangle \langle\,\text{⦚⦚}\,| + |\,\text{⊟}\,\rangle \langle\,\text{⊟}\,|] \,, \quad (1)$$

where the sum is over all plaquettes (faces) of the lattice. At the RK point, when $J = V$, the exact ground state is solvable and is a uniform superposition of all possible dimer configurations. However, in order to witness the rich phenomena arising in weighted classical dimer models, we seek to construct a generalized RK Hamiltonian whose ground state is a weighted superposition of all possible dimer configurations.

Exact Hamiltonian for weighted dimer coverings— In this section, we engineer a Hamiltonian whose exact ground state can be determined and has dimer coverings appearing with amplitudes proportional to a product of the edge weights. For simplicity, we start with the square lattice, but the construction can be generalized to any graph with an RK Hamiltonian.

Consider the square lattice and denote its set of edges by $\mathcal{E}$. For an edge $e \in \mathcal{E}$ and a dimer covering $\mathcal{C}$, let $d_e(\mathcal{C})$ denote the dimer number, that is, $d_e(\mathcal{C}) = 1$ if edge e is occupied in the covering $\mathcal{C}$, and 0 otherwise. For each edge e, we assign

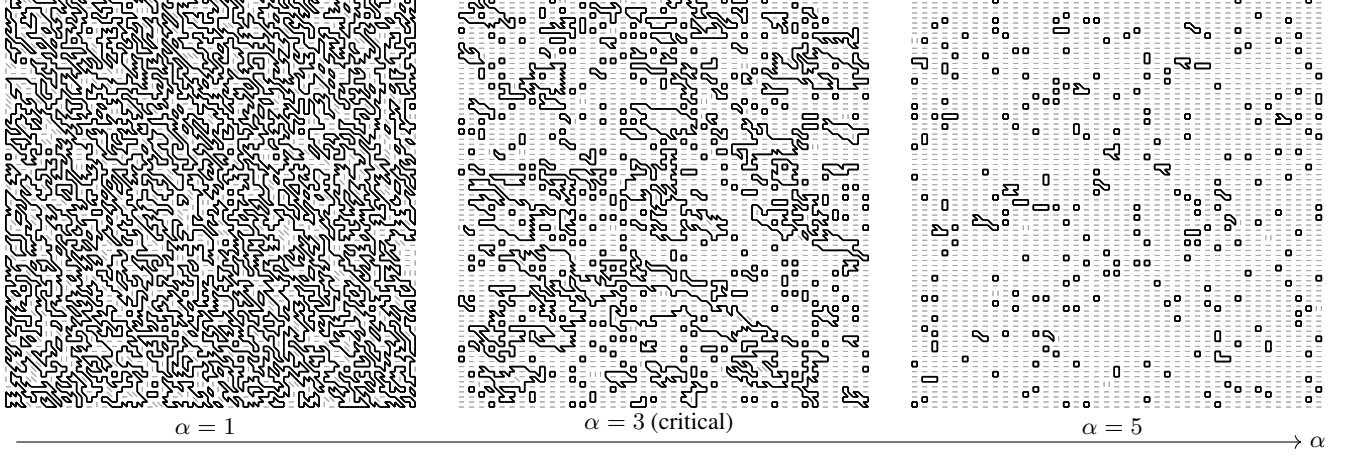$\alpha = 1$ $\alpha = 3$ (critical) $\alpha = 5$ $\to \alpha$

FIG. 1. The quantum dimer model on the weighted triangular lattice as given in Eq. (5) exhibits a continuous quantum phase transition as an edge weight parameter α varies. Statistical behavior in the different phases and at the critical point can be seen through the behavior of random double-dimer coverings in the corresponding *classical* model, shown here for the 2×1 periodic triangular lattice (defined in Fig. 3) with $\alpha = 1$ (left, quantum spin liquid), $\alpha = 3$ (center, critical), and $\alpha = 5$ (right, columnar order), on an 81×81 grid. Double-edges are shown in gray, while loops are shown in black. In the spin liquid phase $\alpha < 3$, the double-dimer covering forms many large macroscopic loops, while in the ordered phase $\alpha > 3$, there are only small loops and double edges. The ordered phase for $\alpha > 3$ is a columnar phase with a nonzero fraction of defects. This loop behavior can be used to intuitively explain the observed vison correlator behavior in the quantum dimer model. The double-dimer coverings are generated using the Kasteleyn matrix method to compute conditional edge probabilities.
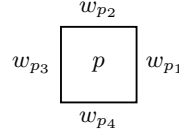

FIG. 2. A plaquette p with surrounding weights w_{p_1}, w_{p_2}, w_{p_3}, and w_{p_4} in a clockwise order.

a weight w_e, which can be a complex number. The weight of a dimer covering $W(\mathcal{C})$ is the product of the weights of all the edges that are occupied by dimers, $W(\mathcal{C}) = \prod_{e \in \mathcal{E}} w_e^{d_e(\mathcal{C})}$. We now construct a Hamiltonian whose ground state is

$$|\psi_{\mathbf{w}}\rangle = \sum_{\mathcal{C}} W(\mathcal{C}) |\mathcal{C}\rangle \, , \qquad (2)$$

where $\mathbf{w}$ is a list of weights w_e. Note that the probability of $\mathcal{C}$ in Eq. (2) is $|W(\mathcal{C})|^2$, rather than $|W(\mathcal{C})|$ which is the standard convention in edge-weighted classical dimer model literature. For convenience, we use the former convention for the general construction. Our edge-weighted RK Hamiltonian having $|\psi_{\mathbf{w}}\rangle$ as a ground state is given by:

$$H = -J \sum_{\square} w_{p_2}^* w_{p_4}^* w_{p_1} w_{p_3} |\mathbin{\vcenter{\hbox{$\scriptstyle\parallel$}}}\rangle\langle\mathbin{\vcenter{\hbox{$\scriptstyle=$}}}| + \text{h.c.}$$

$$+ V \sum_{\square} |w_{p_2} w_{p_4}|^2 |\mathbin{\vcenter{\hbox{$\scriptstyle\parallel$}}}\rangle\langle\mathbin{\vcenter{\hbox{$\scriptstyle\parallel$}}}| + |w_{p_1} w_{p_3}|^2 |\mathbin{\vcenter{\hbox{$\scriptstyle=$}}}\rangle\langle\mathbin{\vcenter{\hbox{$\scriptstyle=$}}}| \, , \quad (3)$$

where the sum is over all the square plaquettes p, with p_i for $i \in \{1, 2, 3, 4\}$ denoting the four edges of p taken in a clockwise order (see Fig. 2). For $J = V$, analogous to the RK

point of Eq. (1), the Hamiltonian turns into a sum of (non-commuting) projectors $H = J \sum_{\square} P_{\square}$, where

$$P_{\square} = \left[w_{p_2}^* w_{p_4}^* |\mathbin{\vcenter{\hbox{$\scriptstyle\parallel$}}}\rangle - w_{p_1}^* w_{p_3}^* |\mathbin{\vcenter{\hbox{$\scriptstyle=$}}}\rangle \right] \left[w_{p_2} w_{p_4} \langle\mathbin{\vcenter{\hbox{$\scriptstyle\parallel$}}}| - w_{p_1} w_{p_3} \langle\mathbin{\vcenter{\hbox{$\scriptstyle=$}}}| \right] .$$
$$(4)$$

It is easy to see that $P_{\square}^2 = \left[|w_{p_2} w_{p_4}|^2 + |w_{p_1} w_{p_3}|^2 \right] P_{\square}$, implying $P_{\square}$ is a projector up to a positive scalar factor. This immediately implies that all the eigen-energies must be non-negative. Moreover, it can be explicitly checked that $P_{\square} |\psi_{\mathbf{w}}\rangle = 0$, for all $P_{\square}$. Thus $|\psi_{\mathbf{w}}\rangle$ is a ground state of H. Note that this construction is very general and applies to any configuration of weights, which need not be translationally invariant. It is worth noting that $|\psi_{\mathbf{w}}\rangle$ is not necessarily the unique ground state for an arbitrary graph. However, since any two dimer coverings of the rectangular grid or Aztec diamond (or more generally any simply connected finite region of the square lattice) are connected by ring flips [47], the ground state of H is *unique* as long as none of the weights are zero. Any diagonal observable calculated in $|\psi_{\mathbf{w}}\rangle$ will be equal to the observable calculated in a classical dimer model with covering weights proportional to $|W(\mathcal{C})|^2$. We can thus use results and techniques for weighted classical dimer models to draw conclusions about the quantum dimer model defined above.

Weighted dimer Hamiltonian for the triangular lattice— Similar to the square lattice Hamiltonian, we can write a Hamiltonian on the triangular lattice. The only modification is that we sum over three kinds of plaquettes. The edge weights we consider are 2×1 periodic, i.e., they are 2-periodic in the horizontal direction and 1-periodic in the vertical direction. This allows for six distinct edge weights, two for each of the

orientations horizontal, vertical, and diagonal. For simplicity, we shall take one horizontal edge weight to be $\alpha \geq 0$, and all five other edge weights to be 1 (see Figs. 3 and 4). For these weights, the explicit Hamiltonian using the above construction is:

$$H = \sum_{\text{even }\square} \mathcal{P}\left(\left|\begin{smallmatrix}\cdot&\cdot\\\cdot&\cdot\end{smallmatrix}\right\rangle - \left|\begin{smallmatrix}\cdot&\cdot\\\cdot&\cdot\end{smallmatrix}\right\rangle\right) + \sum_{\text{odd }\square} \mathcal{P}\left(\alpha\left|\begin{smallmatrix}\cdot&\cdot\\\cdot&\cdot\end{smallmatrix}\right\rangle - \left|\begin{smallmatrix}\cdot&\cdot\\\cdot&\cdot\end{smallmatrix}\right\rangle\right)$$
$$+ \sum_{\diagdown} \mathcal{P}\left(\sqrt{\alpha}\left|\begin{smallmatrix}\diagdown\\\end{smallmatrix}\right\rangle - \left|\begin{smallmatrix}\diagdown\\\end{smallmatrix}\right\rangle\right) + \sum_{\diagdown} \mathcal{P}\left(\left|\begin{smallmatrix}\diagdown\end{smallmatrix}\right\rangle - \left|\begin{smallmatrix}\diagdown\end{smallmatrix}\right\rangle\right), \quad (5)$$

where we use the notation $\mathcal{P}(|\psi\rangle) \equiv |\psi\rangle\langle\psi|$ and the first sum is over square plaquettes having all edge weights 1 while the second sum is over square plaquettes having horizontal edge weights α. The edge weight $\sqrt{\alpha}$ is used in the Hamiltonian so that correlations in the ground state are given by correlations of the classical model with weight α.

Topological phase transition on the triangular lattice— In contrast to quantum dimer models considered on bipartite lattices [2, 48, 49], the RK quantum dimer model on the unweighted triangular lattice is known to be in a $\mathbb{Z}_2$ quantum spin liquid phase [2, 3, 5, 6]. By considering non-uniform edge weights on the triangular lattice, we show that the quantum dimer model defined in Eq. (5) undergoes a topological phase transition from a $\mathbb{Z}_2$ quantum spin liquid to a columnar ordered phase.

The 2×1 periodic weights on the triangular lattice were first introduced and studied for the *classical* dimer model in Ref. [50], where the authors studied the amoebas and geometry of the magnetically-altered Kasteleyn matrix [35], showing an associated Chern number change indicates a classical phase transition at $\alpha = 3$, although the nature of the phases and type of phase transition are not explored. In this Letter, we consider the *quantum* dimer model on the 2×1 periodic triangular lattice, and show that the model undergoes a quantum phase transition, characterized by the *vison* correlator, across $\alpha = 3$. We note by construction the quantum dimer model
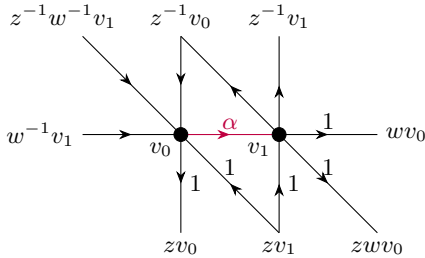

FIG. 3. Fundamental domain and Kasteleyn orientation for the 2×1 periodic triangular lattice with one horizontal edge weight α and all five other weights equal to 1. Horizontal and vertical translates of the fundamental domain are indexed by variables $w, z \in \mathbb{C}$.

of Eq. (5) is exactly solvable, including through the transition point $\alpha = 3$: The exact ground state is given by Eq. (2), and all

correlators can be expressed exactly in terms of the associated Kasteleyn matrix [30–33] (a specific weighted adjacency matrix; see Supplemental Material) and its inverse [32, 33, 51–53]. In particular, the dimer-dimer and vison correlators in Eqs. (6) and (9), which identify the quantum phase, have exact expressions which can be studied analytically as well as evaluated numerically to high (even arbitrary [54–57]) precision. The dimer-dimer correlator $C_{\mu\nu}^d$ is defined as

$$C_{\mu\nu}^d = \langle d_\mu d_\nu \rangle - \langle d_\mu \rangle \langle d_\nu \rangle, \quad (6)$$

where μ and ν label edges of the graph. Writing $\mu = (\mu_0, \mu_1)$ and $\nu = (\nu_0, \nu_1)$ in terms of the corresponding vertices, $C_{\mu\nu}^d$ can be expressed in terms of the Kasteleyn matrix K as [52, 53, 58]

$$C_{\mu\nu}^d = K_{\mu_0,\mu_1} K_{\nu_0,\nu_1} \left(-K_{\mu_0\nu_0}^{-1} K_{\mu_1\nu_1}^{-1} + K_{\mu_0\nu_1}^{-1} K_{\mu_1\nu_0}^{-1} \right). \quad (7)$$

Similarly as in the bipartite planar case [34, 35], one can show the entries of K^{-1} in the infinite size periodic limit are given by double integrals of the form

$$K_{z_0 z_1}^{-1} = \int_0^{2\pi} \int_0^{2\pi} \frac{q_{z_0,z_1}(e^{ik_x}, e^{ik_y})}{P(e^{ik_x}, e^{ik_y})} \frac{dk_x}{2\pi} \frac{dk_y}{2\pi}, \quad (8)$$

where q_{z_0,z_1} is a polynomial depending on the points z_0, z_1, and $P(e^{ik_x}, e^{ik_y})$ is the characteristic polynomial, equivalently the product of band dispersions in the free-fermion picture, for the lattice. This leads to an exact asymptotic expression in terms of sums and products of explicit integrals for any correlator, which allows for analytic study of correlators [34, 35, 57, 59, 60]. In particular, for this model we analytically show (see Supplemental Material) that the dimer-dimer correlations decay exponentially off of the critical point at $\alpha = 3$. More generally, in the full six parameter edge weights case, the dimer-dimer correlator decays exponentially away from the set where one of the horizontal or diagonal edge weights is equal to the sum of the other three remaining such weights.

Quantum dimer models can be mapped to gauge theories, in particular the model studied here can be mapped to a $\mathbb{Z}_2$ gauge theory [20]. Monomers (sites without any dimers touching it) and visons correspond to the electric and magnetic charges under such mapping. Exponential decay of all dimer-dimer correlators and vison correlators implies that the system is gapped and is a $\mathbb{Z}_2$ quantum spin liquid [8, 21, 22, 61]. The vison correlator, which is a nonlocal string operator, can be written in terms of K and K^{-1} as follows. For a fixed path γ between faces f_1 and f_2 (Fig. 4), consider the edges E crossed by γ, and count the number of dimers present in E. The vison correlator between f_1 and f_2 is $|\langle(-1)^{\#\{\text{dimers in } E\}}\rangle|$, and can be written in terms of the Kasteleyn matrix as [57]

$$\left|\langle(-1)^{\#\{\text{dimers in } E\}}\rangle\right| = \sqrt{\det\left(I_{2|E|} - 2(K')_E(K^{-1})_E\right)}, \quad (9)$$

where $I_{2|E|}$ is the $2|E| \times 2|E|$ identity matrix, $(K^{-1})_E$ is the restriction of K^{-1} to E (i.e. to the $2|E|$ vertex indices associated with E) and $(K')_E$ is a restricted Kasteleyn matrix with nonzero entries only for edges in E.
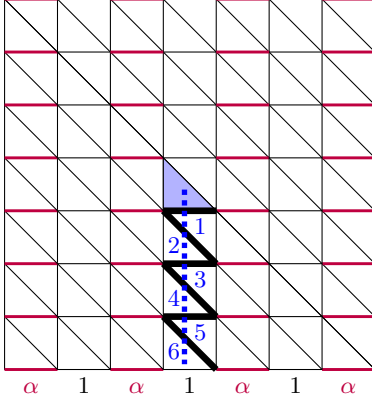

FIG. 4. Path in the triangular lattice for the dimer-dimer and vison correlator calculations. For the vison correlator, the starting face is shaded, with the "face distance" for faces in the path labeled. We count the number of dimers crossed by the dashed path from the starting face to the ending face. The relevant edges to count are shown in bold. For the lattice sizes used in the numerics, this path goes through the horizontal edges with weight 1. The dimer-dimer and vison correlators behave similarly on the adjacent vertical path which goes through the edges with weight α, as well on horizontal paths.

Having defined the relevant correlators and discussed their exact expressions, we plot them in Figs. 5 and 6, and summarize the quantum phases of our model as a function of the parameter α as follows. For $\alpha < 3$, the dimer-dimer and vison correlators decay exponentially, indicating a $\mathbb{Z}_2$ quantum spin liquid phase. For $\alpha = 3$, the correlators are critical. For $\alpha > 3$, the dimer-dimer correlator decays exponentially, but the vison correlator is constant, indicating a trivial ordered phase. The analytic derivations of the exponential decay of the dimer-dimer correlator as well as the analytic estimates of the real space Green's function correlation lengths are given in the Supplemental Material. The diverging correlation lengths for the dimer-dimer and vison correlators near the transition point are shown in Fig. 7. The critical exponents $\beta = 1/8$ and $\nu = 1$ for the transition, which are consistent with the 2D Ising universality class, are obtained via the finite-size scaling numerics up to lattice size 1001×1001 in Fig. 8.

All correlator calculations are performed using the Kasteleyn matrix method (with standard floating point sparse LU methods to calculate entries of K^{-1}), using exact expressions Eqs. (7) and (9) for the correlators. We emphasize that while we present many finite-size numerical results in this section, by Eq. (8) we also obtain exact formulas for all correlators in the infinite-size limit, which are given in terms of products and sums of explicit integrals. For example, the real space Green's function or entries of K^{-1} between two vertically separated points 0 and y in the infinite-size limit can be explicitly written
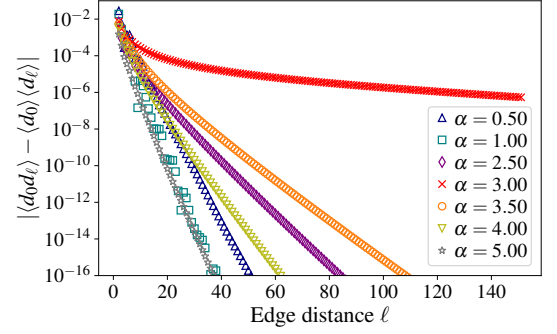

FIG. 5. Dimer-dimer correlator for different values of α, calculated along the path shown in Fig. 4 on a 303×303 size grid. The path starts in the center and ends roughly midway to the boundary. As we show analytically, the dimer-dimer correlator exhibits exponential decay for all values of $\alpha \neq 3$.

as

$$
\langle 0 | K^{-1} | y \rangle = \\
\frac{\pm i}{4\pi^2} \int_0^{2\pi} \int_0^{2\pi} \frac{2\sin(k_y) e^{-ik_y y}\, dk_x\, dk_y}{4\sin^2 k_y + |\alpha - e^{ik_y} - e^{-ik_x} - e^{-ik_x}e^{-ik_y}|^2},
\tag{10}
$$

with the sign depending on the column parity. The integral can also be turned into a single integral using contour integration. Sums and products of such integrals determine all correlations in the infinite-size limit, including dimer-dimer and vison correlators as seen by Eqs. (7) and (9).

Using this, we analytically obtain exponential decay of dimer-dimer correlators off of the critical point, equivalent to the presence of a band gap in the fermion model. Additionally, we can analytically identify the divergence of the correlation length for K^{-1}, equivalently for the real-space Green's function in the free-fermion picture, as $\alpha \to 3$. As detailed in the Supplemental Material, we analytically obtain the Green's function correlation length along a vertical path as

$$
\xi_{\mathrm{G}} \propto \frac{1}{|\alpha - 3|}, \quad \text{as } \alpha \to 3.
\tag{11}
$$

The numerical results in Fig. 7 also show that as $\alpha \to 3$, $\xi_{\mathrm{dimer}} \propto |\alpha - 3|^{-1}$ and $\xi_{\mathrm{vison}} \propto (3 - \alpha)_+^{-1}$, where $(x)_+ = \max(0, x)$. For $\alpha > 3$, the vison correlator is constant so the correlation length is ∞. For the Green's function and dimer-dimer correlator, as $\alpha \to \infty$, $\xi_{\mathrm{G}}, \xi_{\mathrm{dimer}} \propto \frac{1}{\log \alpha} \to 0$, as dimers become more frozen. Regarding the vison correlator, we note that it may be possible to analytically investigate the constant vison correlator values using the methods of Ref. [59]. A simpler vison correlator constant was evaluated for the (uniform) RK dimer model on the square-octagon lattice in Ref. [57].

To understand the nature of the phases and explain the constant vison correlator, we consider double-dimer coverings (see Fig. 1); that is, the union $C \cup C'$ of two independent
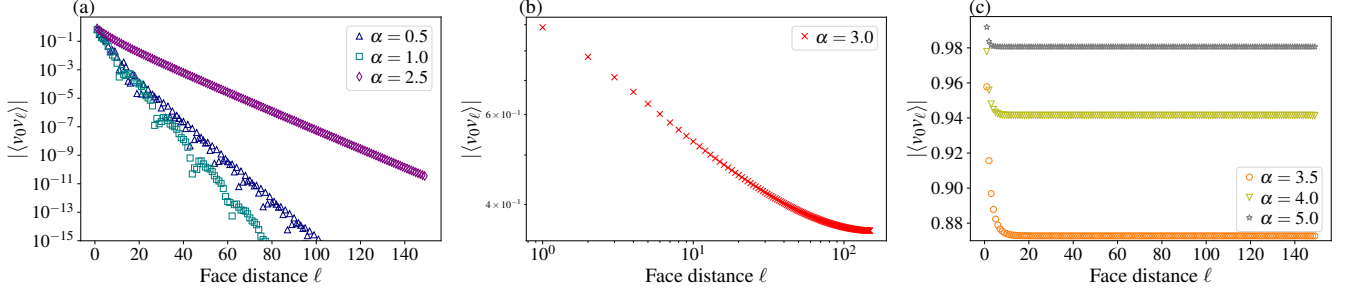
FIG. 6. Vison correlator for different values of α, calculated along the path shown in Fig. 4 on a 303×303 size lattice. The path starts in the center and ends roughly midway to the boundary. (a) The vison correlator decays exponentially for $\alpha < 3$, signaling a spin liquid phase. (b) At the critical value it exhibits power-law decay. (c) The vison correlator is constant for $\alpha > 3$, identifying a trivial ordered phase. In all three regimes, correlators for the adjacent vertical path and a horizontal path (not shown) demonstrate similar decay or lack thereof, with some periodic differences mostly depending on the parity of the path distance.

FIG. 7. Inverse correlation lengths for the dimer-dimer and vison correlators across a vertical and horizontal path for system size 303×303, showing linear behavior near $\alpha = 3$. The inverse correlation length is calculated with respect to the edge or face distance, which is half the coordinate or lattice. The labeled vertical path goes through horizontal edges with weight 1, but the values for the adjacent path through edges with weight α behave similarly.
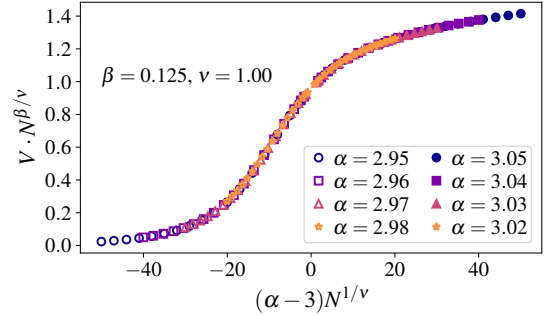

FIG. 8. Finite-size scaling for $V = \sqrt{|\langle v_0 v_\ell \rangle|}$, where $|\langle v_0 v_\ell \rangle|$ is the vison correlator, at lattice distance $\ell \sim N/4$ (halfway from the center to the edge). The path is the vertical path through weight α horizontal edges starting in the center, and calculated for system sizes $N = 41, 61$, and 101 through 1001 by 60s. The curve collapse occurs for $\beta = 1/8$ and $\nu = 1$ as shown.

random dimer coverings C, C'. Since each vertex will have two edges present, the double-dimer covering consists only of loops and double edges. For critical bipartite lattices, the double-dimer model is expected to behave as the Conformal Loop Ensemble CLE_4 [62–64]. Here we are primarily interested in understanding the vison correlator in the non-critical spin liquid or ordered phases. The vison correlator can be expressed in terms of the double-dimer coverings $C \cup C'$ as

$$|\langle f_0 f_\ell \rangle|^2 = \langle (-1)^{\# \text{ dimers in } C \cup C' \text{ along } \gamma} \rangle, \qquad (12)$$

where γ is a path from face f_0 to f_ℓ. Since crossing a double edge does not change the dimer parity, the vison correlator can be written in terms of the number of loops in $C \cup C'$ surrounding each endpoint of γ. As seen in Fig. 1, in the quantum spin liquid phase, loops are large and complicated, allowing for many changes in parity along a vison path. In contrast, in the trivial ordered phase, loops are small and not very common, appearing similar to numerical simulations of the smooth or gaseous phase of bipartite periodic lattices [35]. This sparse loop behavior can be argued to produce a constant vison cor-

relator, as explained further in the Supplemental Material.

Conclusion— In this Letter, we generalized the quantum dimer construction of Rokhsar and Kivelson [1] to construct quantum dimer Hamiltonians whose ground state at the RK point is an arbitrary edge-weighted superposition of dimer coverings. Using this construction, we then demonstrated the existence of an exactly solvable topological phase transition in the weighted quantum dimer model on the triangular lattice, from a $\mathbb{Z}_2$ quantum spin liquid phase to a columnar ordered phase. We used both analytical and numerical results to identify the quantum phases using the real space Green's function, dimer-dimer correlator, and vison correlator. We also noted that all correlators have exact expressions in terms of sums and products of explicit integrals in the infinite-size periodic-boundary limit. Furthermore, we identified critical exponents $\beta = 1/8$ and $\nu = 1$, which are consistent with those of the 2D Ising universality class.

This work opens several new directions for future research on quantum phase transitions, topological phases, and statistics of dimer models. A natural question is to study the model away from the RK point, and to investigate the behavior and

universality class of the phase transition there. Another direction is to develop a general theory and classification for non-bipartite dimer models, which does not yet exist in comparison to the theory for bipartite models [35]. Further study of the behavior of weighted quantum dimer models at the exactly solvable RK point is also a promising direction, in particular it would be interesting to identify all possible phases and topological orders that one can obtain with such models, for example in the direction of double semion phases investigated in Refs. [65, 66], or using the full six parameters in the 2×1 model (or more general models).

[1] D. S. Rokhsar and S. A. Kivelson, Superconductivity and the Quantum Hard-Core Dimer Gas, Phys. Rev. Lett. **61**, 2376 (1988).

[2] R. Moessner and K. S. Raman, Quantum dimer models, in *Introduction to Frustrated Magnetism: Materials, Experiments, Theory* (Springer Berlin Heidelberg, Berlin, Heidelberg, 2011) pp. 437–479.

[3] R. Moessner and S. L. Sondhi, Resonating Valence Bond Phase in the Triangular Lattice Quantum Dimer Model, Phys. Rev. Lett. **86**, 1881 (2001).

[4] R. Moessner, S. L. Sondhi, and P. Chandra, Phase diagram of the hexagonal lattice quantum dimer model, Phys. Rev. B **64**, 144416 (2001).

[5] G. Misguich and F. Mila, Quantum dimer model on the triangular lattice: Semiclassical and variational approaches to vison dispersion and condensation, Phys. Rev. B **77**, 134421 (2008).

[6] A. Ioselevich, D. A. Ivanov, and M. V. Feigelman, Ground-state properties of the Rokhsar-Kivelson dimer model on the triangular lattice, Phys. Rev. B **66**, 174405 (2002).

[7] T. M. Schlittler, R. Mosseri, and T. Barthel, Phase diagram of the hexagonal lattice quantum dimer model: Order parameters, ground-state energy, and gaps, Phys. Rev. B **96**, 195142 (2017).

[8] L. Balents, M. P. A. Fisher, and S. M. Girvin, Fractionalization in an easy-axis Kagome antiferromagnet, Phys. Rev. B **65**, 224412 (2002).

[9] S. Balasubramanian, V. Galitski, and A. Vishwanath, Classical vertex model dualities in a family of two-dimensional frustrated quantum antiferromagnets, Phys. Rev. B **106**, 195127 (2022).

[10] S. Balasubramanian, D. Bulmash, V. Galitski, and A. Vishwanath, Interplay of symmetry breaking and deconfinement in three-dimensional quantum vertex models, Phys. Rev. B **110**, L180401 (2024).

[11] J. Shah, G. Nambiar, A. V. Gorshkov, and V. Galitski, A quantum monomer-dimer model on Penrose tilings (2025), arXiv:2503.15588.

[12] L. Savary and L. Balents, Quantum spin liquids: A review, Rep. Prog. Phys. **80**, 016502 (2017).

[13] M. Hermele, M. P. A. Fisher, and L. Balents, Pyrochlore photons: The $U(1)$ spin liquid in a $S = 1/2$ three-dimensional frustrated magnet, Phys. Rev. B **69**, 064404 (2004).

[14] R. Moessner and S. L. Sondhi, Ising and dimer models in two and three dimensions, Phys. Rev. B **68**, 054405 (2003).

[15] A. Kitaev, Anyons in an exactly solved model and beyond, Ann. Phys. **321**, 2 (2006), arxiv:cond-mat/0506438.

[16] A. Kitaev, Fault-tolerant quantum computation by anyons, Annals of Physics **303**, 2 (2003).

[17] X.-G. Wen, Quantum orders and symmetric spin liquids, Phys. Rev. B **65**, 165113 (2002).

[18] X.-G. Wen, *Quantum Field Theory of Many-Body Systems: From the Origin of Sound to an Origin of Light and Electrons* (Oxford University Press, 2007).

[19] M. A. Levin and X.-G. Wen, String-net condensation: A physical mechanism for topological phases, Phys. Rev. B **71**, 045110 (2005).

[20] R. Moessner, S. L. Sondhi, and E. Fradkin, Short-ranged resonating valence bond physics, quantum dimer models, and Ising gauge theories, Phys. Rev. B **65**, 024504 (2001).

[21] T. Senthil and M. P. A. Fisher, Fractionalization, topological order, and cuprate superconductivity, Phys. Rev. B **63**, 134521 (2001).

[22] T. Senthil and M. P. A. Fisher, Fractionalization in the cuprates: Detecting the topological order, Phys. Rev. Lett. **86**, 292 (2001).

[23] G. Misguich, D. Serban, and V. Pasquier, Quantum dimer model on the Kagome lattice: Solvable dimer-liquid and Ising gauge theory, Phys. Rev. Lett. **89**, 137202 (2002).

[24] A. M. Essin and M. Hermele, Classifying fractionalization: Symmetry classification of gapped F_2 spin liquids in two dimensions, Phys. Rev. B **87**, 104406 (2013).

[25] G. Semeghini, H. Levine, A. Keesling, S. Ebadi, T. T. Wang, D. Bluvstein, R. Verresen, H. Pichler, M. Kalinowski, R. Samajdar, A. Omran, S. Sachdev, A. Vishwanath, M. Greiner, V. Vuletić, and M. D. Lukin, Probing topological spin liquids on a programmable quantum simulator, Science **374**, 1242 (2021).

[26] R. Verresen, M. D. Lukin, and A. Vishwanath, Prediction of Toric Code Topological Order from Rydberg Blockade, Phys. Rev. X **11**, 031005 (2021).

[27] J. Shah, G. Nambiar, A. V. Gorshkov, and V. Galitski, Quantum Spin Ice in Three-Dimensional Rydberg Atom Arrays, Phys. Rev. X **15**, 011025 (2025).

[28] Z. Zeng, G. Giudici, and H. Pichler, Quantum dimer models with Rydberg gadgets, Phys. Rev. Res. **7**, L012006 (2025).

[29] Z. Yan, R. Samajdar, Y.-C. Wang, S. Sachdev, and Z. Y. Meng, Triangular lattice quantum dimer model with variable dimer density, Nat. Commun. **13**, 5799 (2022).

[30] P. W. Kasteleyn, The statistics of dimers on a lattice: I. the number of dimer arrangements on a quadratic lattice, Physica **27**, 1209 (1961).

[31] P. W. Kasteleyn, Dimer statistics and phase transitions, J. Math. Phys. **4**, 287 (1963).

[32] H. N. Temperley and M. E. Fisher, Dimer problem in statistical mechanics-an exact result, Phil. Mag. **6**, 1061 (1961).

[33] M. E. Fisher, Statistical mechanics of dimers on a plane lattice, Phys. Rev. **124**, 1664 (1961).

[34] H. Cohn, R. Kenyon, and J. Propp, A variational principle for domino tilings, J. Amer. Math. Soc. **14**, 297 (2001).

[35] R. Kenyon, A. Okounkov, and S. Sheffield, Dimers and amoebae, Ann. of Math. (2) **163**, 1019 (2006).

[36] C. Boutillier, Pattern densities in non-frozen planar dimer models, Comm. Math. Phys. **271**, 55 (2007).

[37] R. Kenyon, Lectures on Dimers (2009), arXiv:0910.3129.

[38] S. Chhita, K. Johansson, and B. Young, Asymptotic domino statistics in the Aztec diamond, Ann. Appl. Probab. **25**, 1232 (2015).

[39] S. Chhita and B. Young, Coupling functions for domino tilings of Aztec diamonds, Adv. Math. **259**, 173 (2014).

[40] S. Chhita and K. Johansson, Domino statistics of the two-periodic Aztec diamond, Adv. Math. **294**, 37 (2016).

[41] T. Berggren and M. Duits, Correlation functions for determinantal processes defined by infinite block Toeplitz minors, Adv. Math. **356**, 106766, 48 (2019).

[42] M. Duits and A. B. J. Kuijlaars, The two-periodic Aztec diamond and matrix valued orthogonal polynomials, J. Eur. Math. Soc. (JEMS) **23**, 1075 (2021).

[43] V. Gorin, *Lectures on random lozenge tilings*, Cambridge Studies in Advanced Mathematics, Vol. 193 (Cambridge University Press, Cambridge, 2021) pp. viii+250.

[44] A. Borodin and M. Duits, Biased 2×2 periodic Aztec diamond and an elliptic curve, Probab. Theory and Relat. Fields **187**, 259 (2023).

[45] T. Berggren and A. Borodin, Geometry of the doubly periodic aztec dimer model (2025).

[46] C. Boutillier and B. Tilière, Fock's dimer model on the Aztec diamond, arXiv:2405.20284 (2025).

[47] W. P. Thurston, Conway's tiling groups, Amer. Math. Monthly **97**, 757 (1990).

[48] C. L. Henley, Relaxation time for a dimer covering with height representation, J. Statist. Phys. **89**, 483 (1997).

[49] E. Fradkin, D. A. Huse, R. Moessner, V. Oganesyan, and S. L. Sondhi, Bipartite Rokhsar–Kivelson points and cantor deconfinement, Phys. Rev. B **69**, 224415 (2004).

[50] C. Nash and D. O'Connor, Dimer geometry, amoebae and a vortex dimer model, J. Phys. A **50**, 355002, 30 (2017).

[51] E. W. Montroll, R. B. Potts, and J. C. Ward, Correlations and spontaneous magnetization of the two-dimensional Ising model, J. Math. Phys. **4**, 308 (1963).

[52] R. Kenyon, Local statistics of lattice dimers, Ann. Inst. Henri Poincaré (B) Probab. Stat. **33**, 591 (1997).

[53] P. Fendley, R. Moessner, and S. L. Sondhi, Classical dimers on the triangular lattice, Phys. Rev. B **66**, 214513 (2002).

[54] D. B. Wilson, Determinant algorithms for random planar structures, in *SODA*, Vol. 97 (ACM/SIAM, 1997) pp. 258–267.

[55] H. R. Lee and B. D. Saunders, Fraction free Gaussian elimination for sparse matrices, J. Symb. Comput. **19**, 393 (1995).

[56] G. C. Nakos, P. R. Turner, and R. M. Williams, Fraction-free algorithms for linear and polynomial equations, ACM SIGSAM Bull. **31**, 11 (1997).

[57] J. Shah, L. Shou, J. Shuler, and V. Galitski, Breakdown of the thermodynamic limit in quantum spin and dimer models, arXiv preprint arXiv:2506.15769 (2025).

[58] D. Cimasoni and N. Reshetikhin, Dimers on surface graphs and spin structures. I, Comm. Math. Phys. **275**, 187 (2007).

[59] E. L. Basor and T. Ehrhardt, Asymptotics of block Toeplitz determinants and the classical dimer model, Comm. Math. Phys. **274**, 427 (2007).

[60] E. Basor and P. Bleher, Exact solution of the classical dimer model on a triangular lattice: monomer-monomer correlations, Comm. Math. Phys. **356**, 397 (2017).

[61] T. Senthil and M. P. A. Fisher, Z_2 gauge theory of electron fractionalization in strongly correlated systems, Phys. Rev. B **62**, 7850 (2000).

[62] R. Kenyon, Conformal invariance of loops in the double-dimer model, Comm. Math. Phys. **326**, 477 (2014).

[63] J. Dubédat, Double dimers, conformal loop ensembles and isomonodromic deformations, J. Eur. Math. Soc. (JEMS) **21**, 1 (2019).

[64] M. Basok and D. Chelkak, Tau-functions à la Dubédat and probabilities of cylindrical events for double-dimers and CLE(4), J. Eur. Math. Soc. (JEMS) **23**, 2787 (2021).

[65] Y. Qi, Z.-C. Gu, and H. Yao, Double-semion topological order from exactly solvable quantum dimer models, Phys. Rev. B **92**, 155105 (2015).

[66] O. Buerschaper, S. C. Morampudi, and F. Pollmann, Double semion phase in an exactly solvable quantum dimer model on the kagome lattice, Phys. Rev. B **90**, 195148 (2014).

[67] D. Cimasoni, The geometry of dimer models, Winter Braids Lect. Notes **1**, Exp. No. 2, 14 (2014).

[68] P. W. Kasteleyn, Graph theory and crystal physics, in *Graph Theory and Theoretical Physics*, edited by F. Harary (Academic Press, London, 1967) pp. 43–110.

[69] One could alternatively define a Kasteleyn orientation in terms of clockwise orientation.

[70] If $z \in \{-1, \alpha\}$, then $c_1(z, \alpha) = 0$ and the denominator is simply linear with a zero at $w = -c_3(z, \alpha)/c_2(z, \alpha) = 0$. The contour integral over w is then zero for $\ell, j \neq 0$, which agrees with the formulas (28) and (29) for $z \neq -1, \alpha$.

[71] H. Broer and F. Takens, *Dynamical systems and chaos*, Applied Mathematical Sciences, Vol. 172 (Springer, New York, 2011) pp. xvi+313.

[72] V. I. Arnol'd, *Geometrische Methoden in der Theorie der gewöhnlichen Differentialgleichungen* (Birkhäuser Verlag, Basel, 1987) p. 320, translated from the Russian by Ernst Günter Giessmann, Bernd Graw and Horst Theel.

[73] M. E. Fisher and J. Stephenson, Statistical mechanics of dimers on a plane lattice. II. dimer correlations and monomers, Phys. Rev. **132**, 1411 (1963).

[74] R. Kenyon, Height fluctuations in the honeycomb dimer model, Comm. Math. Phys. **281**, 675 (2008).

[75] C. Boutillier, D. Cimasoni, and B. de Tilière, Minimal bipartite dimers and higher genus Harnack curves, Probab. Math. Phys. **4**, 151 (2023).

Supplemental Material

CONTENTS

Review of Kasteleyn's method

In this section, we briefly review the Kasteleyn matrix and some of its properties. For further references, see e.g. Refs. [30, 37, 43, 67]. For a planar graph, one can always define a Kasteleyn orientation [30, 53, 67, 68], which can be defined as an assignment of directions to the edges so that the number of edges oriented counterclockwise around each face is odd [69]. For each directed edge $(v_1 \to v_2)$ between two vertices in the graph, we assign a positive orientation if it agrees with the Kasteleyn orientation and a negative orientation if it disagrees. Recall we consider edge weights $w(v_1, v_2) = w(v_2, v_1)$ assigned to the edges of the graph. The Kasteleyn matrix K is a weighted, signed adjacency matrix which can be defined as:

$$K(v_1, v_2) = \begin{cases} w(v_1, v_2), & (v_1 \to v_2) \text{ has positive orientation} \\ -w(v_1, v_2) & (v_1 \to v_2) \text{ has negative orientation} \\ 0, & (v_1, v_2) \text{ is not an edge} \end{cases} \tag{13}$$

Note that K is skew-symmetric. If the graph is bipartite, then K has a block structure and one can instead consider half-size Kasteleyn matrices where the rows and columns are indexed by one of the two sets of vertices. Since we work on the triangular lattice, we will however have to use the full size matrix defined in (13).

For a dimer configuration $\mathcal{C}$, the weight $\mathcal{W}(\mathcal{C}) = \prod_{e \in \mathcal{E}} w_e^{d_e(\mathcal{C})}$ is the product of all edge weights of dimers in $\mathcal{C}$. By construction of the Kasteleyn orientation, the partition function can be written as [30–33, 68]

$$Z \equiv \sum_{\mathcal{C}} \mathcal{W}(\mathcal{C}) = |\operatorname{Pf}(K)|, \tag{14}$$

where $\operatorname{Pf}(K)$ denotes the Pfaffian, defined for a $2n \times 2n$ skew-symmetric matrix A as

$$\operatorname{Pf}(A) = \frac{1}{2^n n!} \sum_{\sigma \in S_{2n}} \operatorname{sgn}(\sigma) \prod_{i=1}^{n} A_{\sigma(2i-1),\sigma(2i)}. \tag{15}$$

The Pfaffian is related to the determinant as

$$\operatorname{Pf}(A)^2 = \det A. \tag{16}$$

Since the Pfaffian of a Kasteleyn matrix counts weighted dimer coverings for the corresponding graph, it can be used to calculate dimer probabilities and correlations. To count the number of dimer configurations where a certain set of edges $E = \{e_1, \ldots, e_k\}$, $e_i = (v_i, w_i)$, appear, one takes the Pfaffian of the Kasteleyn matrix for the subgraph with all vertices $V_E = \{v_1, w_1, v_2, w_2, \ldots, v_k, w_k\}$ (and their attached edges) removed. This leads to the Pfaffian form of Kenyon's formula [62], [58, §6.3],

$$\mathbb{P}[e_1, \ldots, e_k \text{ all occur in a dimer covering}] = (-1)^k \left[\prod_{i=1}^{k} K(v_i, w_i) \right] \operatorname{Pf}(K_{V_E}^{-1}), \tag{17}$$

where the Pfaffian is over the $2|E| \times 2|E|$ submatrix of K^{-1} corresponding to the $2|E|$ vertices in V_E. The product $\prod_{i=1}^{k} K(v_i, w_i)$ is just a signed product of the weights for the edges in E.

As an example, (17) gives the dimer-dimer correlator between dimers $\mu = (\mu_0, \mu_1)$ and $\nu = (\nu_0, \nu_1)$ as

$$\langle d_\mu d_\nu \rangle - \langle d_\mu \rangle \langle d_\nu \rangle = K(\mu_0, \mu_1) K(\nu_0, \nu_1) \left[-K^{-1}(\mu_0, \nu_0) K^{-1}(\mu_1, \nu_1) + K^{-1}(\mu_0, \nu_1) K^{-1}(\mu_1, \nu_0) \right]. \tag{18}$$

Note this formula has an additional term compared to the bipartite case, where the dimer-dimer correlator is proportional to a single product of the Green's function at two points [35]. Equation (17) is also used to derive the vison correlator expression (9) following [57, §II.B] and using (16).

Exponential decay and correlation lengths off the critical point

To study exponential decay and correlation lengths analytically, we consider the infinite size periodic limit, i.e. the lattice is given periodic boundary conditions and then the size is taken to infinity. As noted in (8) of the main text, in this setting it is well-known that the entries of an infinite limit K^{-1} are given in terms of double integrals [34, 35, 53]. To obtain the explicit formulas for the double integrals, we proceed as follows. From the fundamental domain in Fig. 3, we read off the magnetic Kasteleyn matrix [34, 35], also considered for the weighted triangular lattice in [50], as

$$K_1(w, z) = \begin{bmatrix} z - z^{-1} & \alpha - z - w^{-1} - z^{-1} w^{-1} \\ -\alpha + w + z^{-1} + zw & -(z - z^{-1}) \end{bmatrix}. \tag{19}$$

The inverse is

$$K_1^{-1}(w, z) = \frac{1}{P(w, z)} \begin{bmatrix} -(z - z^{-1}) & -\alpha + z + w^{-1} + z^{-1} w^{-1} \\ \alpha - w - z^{-1} - zw & z - z^{-1} \end{bmatrix}, \tag{20}$$

where $P(w, z) = \det K_1(w, z) = -(z - z^{-1})^2 + (\alpha - z - w^{-1} - z^{-1} w^{-1})(\alpha - w - z^{-1} - zw)$ is the *characteristic polynomial*. When $w = e^{ik_x}$ and $z = e^{ik_y}$ are on the unit circle, this gives

$$P(e^{ik_x}, e^{ik_y}) = 4 \sin^2 k_y + |\alpha - e^{ik_y} - e^{-ik_x} - e^{-ik_x} e^{-ik_y}|^2, \tag{21}$$

which is also the product of band dispersions for the corresponding free-fermion model.

We index vertices in the triangular lattice by coordinates (x, y, t), where $(x, y) \in \mathbb{Z}^2$ denotes the translation of the fundamental cell, and $t \in \{0, 1\}$ specifies the vertex v_0 or v_1 in Fig. 3. Then in the infinite size periodic limit, (20) implies [34, 35]

$$\langle 0, 0, s | K^{-1} | x, y, t \rangle = \int_0^{2\pi} \int_0^{2\pi} \frac{Q_{st}(e^{ik_x}, e^{ik_y}) e^{-i(k_x x + k_y y)}}{4 \sin^2 k_y + |\alpha - e^{ik_y} - e^{-ik_x} - e^{-ik_x} e^{-ik_y}|^2} \frac{dk_x}{2\pi} \frac{dk_y}{2\pi}, \tag{22}$$

where $Q_{st}(w, z)$ is the rational function given by the (s, t) matrix entries [without $1/P(w, z)$] of (20). See Refs. [34, §7], [53], or [57, Appendix] for similar calculations for K^{-1} on other weighted dimer models.

As before, we consider the correlators in the infinite size periodic limit. The matrix elements of K^{-1} given in Eq. (22) correspond to the 2D Fourier transform of a rational function F whose denominator is given by the product of band dispersions $P(e^{ik_x}, e^{ik_y})$ in Eq. (21). Using that $P(e^{ik_x}, e^{ik_y})$ is a sum of two nonnegative terms, we see it can only be zero if $k_y = k_x = 0$ and $\alpha = 3$. In particular, for $\alpha \neq 3$, there is a band gap since $P(e^{ik_x}, e^{ik_y}) \neq 0$ for all $k_x, k_y \in [0, 2\pi]$, and analyticity of the resulting function F implies exponential decay of its Fourier transform, and hence of the matrix elements of K^{-1}. As a result, using the expression (18) for the dimer-dimer connected correlator in terms of the entries of K^{-1} shows we must have exponential decay for $\alpha \neq 3$,

$$|\langle d_\mu d_\nu \rangle - \langle d_\mu \rangle \langle d_\nu \rangle| \leq C e^{-c \operatorname{dist}(\mu, \nu)}, \tag{23}$$

where C, c may depend on α, and $\operatorname{dist}(\mu, \nu)$ denotes some distance (such as Euclidean distance) on the lattice.

Next, for $\alpha \neq 3$, we calculate the correlation length ξ_G for the inverse Kasteleyn limit, which corresponds to the real-space Green's function in the corresponding free-fermion model, along a vertical path. We start with the infinite size periodic limit formula (22), which gives expressions of the form

$$\int_0^{2\pi} \int_0^{2\pi} \frac{e^{ijk_x} e^{i\ell k_y}}{4 \sin^2 k_y + |\alpha - e^{ik_y} - e^{-ik_x} - e^{-ik_x} e^{-ik_y}|^2} \frac{dk_x}{2\pi} \frac{dk_y}{2\pi}$$
$$= \frac{1}{(2\pi i)^2} \oint_{S^1} \oint_{S^1} \frac{w^j z^\ell}{c_1(z, \alpha) w^2 + c_2(z, \alpha) w + c_3(z, \alpha)} \, dw \, \frac{dz}{z}, \tag{24}$$

where

$$c_1(z,\alpha) = (z-\alpha)(z+1)$$
$$c_2(z,\alpha) = 5 + \alpha^2 - (z^2 + z^{-2}) + (1-\alpha)(z + z^{-1}) \tag{25}$$
$$c_3(z,\alpha) = (z^{-1}-\alpha)(z^{-1}+1)$$

The denominator of the integrand factors as $c_1(z,\alpha)w^2 + c_2(z,\alpha)w + c_3(z,\alpha) = c_1(z,\alpha)[w - r_+(z,\alpha)][w - r_-(z,\alpha)]$ for

$$r_\pm(z,\alpha) = \frac{-c_2(z,\alpha) \pm \sqrt{c_2(z,\alpha)^2 - 4c_1(z,\alpha)c_3(z,\alpha)}}{2c_1(z,\alpha)}, \tag{26}$$

for $z \neq -1, \alpha$ [70]. For $z = e^{ik_y}$ with $k_y \in \mathbb{R}$, we have

$$|r_+(z,\alpha)r_-(z,\alpha)| = \frac{|c_2(z,\alpha)^2 - (c_2(z,\alpha)^2 - 4c_1(z,\alpha)c_3(z,\alpha)|)}{4|c_1(z,\alpha)|^2} = \frac{|c_3(z,\alpha)|}{|c_1(z,\alpha)|} = 1. \tag{27}$$

Also, $c_2(e^{ik_y}, \alpha)$ is real and is > 0, so we see that $|r_+(e^{ik_y}, \alpha)| \leq |r_-(e^{ik_y}, \alpha)|$. We know there are no zeros of the denominator of the integrand in (24) for any $|z| = |w| = 1$ iff $\alpha \neq 3$. Thus for $\alpha \neq 3$, we must have $|r_+(z,\alpha)| < 1$ and $|r_-(z,\alpha)| > 1$ for all $|z| = |w| = 1$. Therefore, for $j \geq 0$ and $\alpha \neq 3$, the only pole inside the unit circle is at $w = r_+(z,\alpha)$, and the residue theorem implies

$$\frac{1}{(2\pi i)^2} \oint_{S^1} \frac{z^\ell \, dz}{z} \oint_{S^1} \frac{w^j}{c_1(z,\alpha)[w - r_+(z,\alpha)][w - r_-(z,\alpha)]} \, dw = \int_0^{2\pi} \frac{\left[r_+(e^{ik_y},\alpha)\right]^j e^{i\ell k_y}}{c_1(z,\alpha)[r_+(e^{ik_y},\alpha) - r_-(e^{ik_y},\alpha)]} \frac{dk_y}{2\pi}$$
$$= \int_0^{2\pi} \frac{\left[r_+(e^{ik_y},\alpha)\right]^j e^{i\ell k_y}}{\sqrt{c_2(e^{ik_y},\alpha)^2 - 4c_1(e^{ik_y},\alpha)c_3(e^{ik_y},\alpha)}} \frac{dk_y}{2\pi}. \tag{28}$$

We consider the decay along a vertical path in the triangular lattice. For example, we can consider fixed $j \geq 0$, and replace $e^{i\ell k_y}$ in the numerator with $\sin(k_y)e^{i\ell k_y}$; up to constant factors this corresponds to the Green's function between two points separated vertically. The integral (28), with modified numerator, is then the Fourier transform of the function

$$f_a(k_y) = \frac{2\sin(k_y)c_1(e^{ik_y},\alpha)\left[r_+(e^{ik_y},\alpha)\right]^j}{\sqrt{c_2(e^{ik_y},\alpha)^2 - 4c_1(e^{ik_y},\alpha)c_3(e^{ik_y},\alpha)}}, \tag{29}$$

for $k_y \in \mathbb{R}/(2\pi\mathbb{Z})$. The rate of decay of the Fourier transform of f_a is determined by the nearest complex zero of f_a, due to a Paley–Wiener theorem:

Lemma 1. *If f is 2π-periodic and real analytic with analytic extension to a neighborhood of the strip $\{z \in \mathbb{C} : |\operatorname{Im} z| \leq \kappa\}$ for some $\kappa > 0$, then the Fourier coefficients $\hat{f}(\xi) = \frac{1}{2\pi} \int_0^{2\pi} f(x)e^{-i\xi x} \, dx$ satisfy*

$$|\hat{f}(\xi)| \leq Ce^{-\kappa|\xi|}, \tag{30}$$

for some constant $C = C(f)$. Conversely, if the Fourier coefficients have the above exponential decay, then f has analytic extension to the strip $\{z \in \mathbb{C} : |\operatorname{Im} z| < \kappa\}$.

More generally, a d-dimensional version can be formulated, see for example, Ref. [71, Lemma 5.6], [72].

Therefore to determine the inverse correlation length of K^{-1}, we locate the zeros of $d(e^{ik_y},\alpha) := \sqrt{c_2(e^{ik_y},\alpha)^2 - 4c_1(e^{ik_y},\alpha)c_3(e^{ik_y},\alpha)}$, for $k_y = t + is$, which are closest to the real line.

When $\alpha = 3$, we see that $k_y = 0$ solves $d(e^{ik_y},\alpha)^2 = 0$. When we perturb α away from 3, this root, which is quadratic for $d(e^{ik_y},\alpha)^2$, will split and move into the complex plane. We look for these roots by Taylor expanding $d(e^{i(t+is)},\alpha)^2$ as $s,t \to 0$ and $\alpha \to 3$, which gives to leading orders,

$$d(e^{i(t+is)},\alpha)^2 \asymp (64t^2 + 128its - 64s^2 - 160t^2s^2)[1 + (\alpha - 3)] + (16 + 24t^2 + 48its - 24s^2 + 18t^2s^2)(\alpha - 3)^2. \tag{31}$$

Taking $t = 0$ so the imaginary part of the right hand side is zero, we solve for the smallest zeros of

$$d(e^{-s},\alpha)^2 = -64s^2 - 64s^2(\alpha - 3) + (16 - 24s^2)(\alpha - 3)^2 + O(s^3) + O((\alpha - 3)^3). \tag{32}$$

Dropping higher order terms gives that this is equal to zero for

$$s^2 = \frac{2(\alpha-3)^3}{8 + 8(\alpha-3) + 3(\alpha-3)^2} = \frac{(\alpha-3)^2}{4}(1 + O(\alpha-3)). \tag{33}$$

Moreover, the numerator of (29) is bounded away from zero, since $\sin(k_y)$ has no α dependence, and the other numerator terms were nonzero for $t = s = 0$ and $\alpha = 3$. Thus the distance to the nearest complex zero of $d(e^{ik_y}, \alpha)$ for α near 3 is $|s| \sim \frac{1}{2}|\alpha-3|$. This gives the correlation length for K^{-1} (the real-space Green's function in the free-fermion picture) along a vertical path as

$$\xi_G \sim \frac{2}{|\alpha-3|}, \quad \text{as } \alpha \to 3, \tag{34}$$

measured in lattice distance. One could also study the correlation length along other paths similarly. We plot the inverse correlation lengths along different paths numerically in Fig. 9. In particular, this confirms (34) numerically for the vertical path.
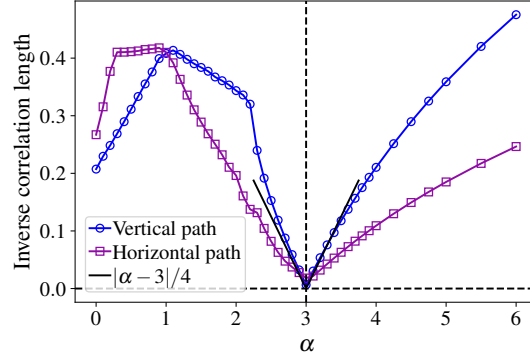

FIG. 9. Inverse correlation lengths ξ_G^{-1} for the inverse Kasteleyn matrix values $|K^{-1}(v_0, v_\ell)|$ (or real-space Greens' function) along a vertical and horizontal path, using lattice size 303×303. The correlation length is calculated with respect to vertices v_ℓ which include all of those in the zigzag path drawn in Fig. 4, in particular alternating between columns (for the vertical path) or rows (for the horizontal path). There are two vertices per lattice square in the zigzag path, accounting for the extra factor of $1/2$ in the comparison to $|\alpha-3|/4$. The inverse correlation lengths are calculated using a best fit regression on vertices $\ell = 40$ to 150, as measured from the center $\ell = 0$ and ending roughly halfway to the edge at the endpoint $\ell = 150$.

For large α, we can show along a horizontal or vertical path that

$$\xi_G \sim \frac{1}{\log\left(\frac{\alpha-1}{2}\right)}, \quad \text{as } \alpha \to \infty. \tag{35}$$

As shown in Fig. 10, the dimer-dimer inverse correlation length behaves similarly as $\xi_{\text{dimer}} \propto \frac{1}{\log\left(\frac{\alpha-1}{2}\right)}$. Starting from the band dispersion $P(e^{ik_x}, e^{ik_y})$ in (21), we see there is a complex zero at $(k_x, k_y) = (0, i\log\left(\frac{\alpha-1}{2}\right))$. This is also not a zero of any of the $Q_{st}(e^{ik_x}, e^{ik_y})$ in (20). A quick standard estimate shows that if $f : (\mathbb{R}/2\pi\mathbb{Z})^d \to \mathbb{C}$ has Fourier coefficients $|\hat{f}(\xi)| \leq Ce^{-\kappa\|\xi\|_2}$, then f has analytic extension to the strip $\{x + iv \in (\mathbb{C}/2\pi\mathbb{Z})^d : \|v\|_2 < \kappa\}$. Thus for $P(e^{ik_x}, e^{ik_y})$, the complex zero prevents analytic extension to $\kappa = \log\left(\frac{\alpha-1}{2}\right)$, which implies $\xi_G^{-1} \leq \log\left(\frac{\alpha-1}{2}\right)$. To obtain a lower bound on ξ_G^{-1}, let $k_x = \theta + iu$ and $k_y = \varphi + iv$. If $|u| + |v| \leq \kappa = (1-\delta)\log\left(\frac{\alpha-1}{2}\right)$, then

$$\begin{aligned}
&|P(e^{i(\theta+iu)}, e^{i(\varphi+iv)})| \\
&= \left|e^{2i\theta}e^{-2u} + e^{-2i\theta}e^{2u} - 2 + (a - e^{-i\varphi}e^v - e^{i\theta}e^{-u} - e^{-i\theta}e^{-i\varphi}e^u e^v)(a - e^{i\varphi}e^{-v} - e^{-i\theta}e^u - e^{i\theta}e^{i\varphi}e^{-u}e^{-v})\right| \\
&\geq (\alpha - 3e^\kappa)^2 - 2 - 2e^{2\kappa} = \alpha^2 - O(\alpha^{2-2\delta}).
\end{aligned} \tag{36}$$

As $\alpha \to \infty$, this is bounded away from zero. Thus there are no complex zeros of P if $|u| + |v| \leq (1-\delta)\log\left(\frac{\alpha-1}{2}\right)$. Then along a horizontal or vertical path, a 2-dimensional version of Lemma 1, which replaces the absolute values with the ℓ^1 norm [71, Lemma 5.6], implies $\xi_G^{-1} \geq (1-\delta)\log\left(\frac{\alpha-1}{2}\right)$ for any $\delta > 0$ and sufficiently large α.

For completeness, we comment on the inverse correlation lengths calculated in Fig. 7 in the Main Text. There, the inverse correlation lengths are calculated using linear regression for edge/face distances starting at 30 and ending at 150 (for dimers) or when numerical precision drops below 10^{-15} (for vison correlator near $\alpha = 1$).
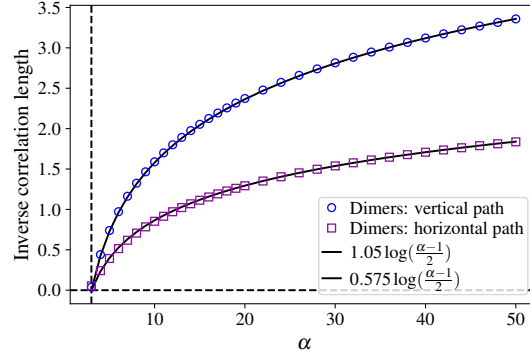
FIG. 10. Dimer-dimer inverse correlation length from $\alpha = 3$ to 50, using lattice size 303×303.

Power-law decay at the critical point

As suggested by Eq. (18), we see numerically in Fig. 11 the dimer-dimer correlator for $\alpha = 3$ decays as power-law as well, although along the horizontal path it appears to decay at a faster power than $1/R^2$. Note that for the square lattice at criticality, it is also known that certain pairs have dimer-dimer correlators that can decay as a power-law faster than $1/R^2$ [37, 73].
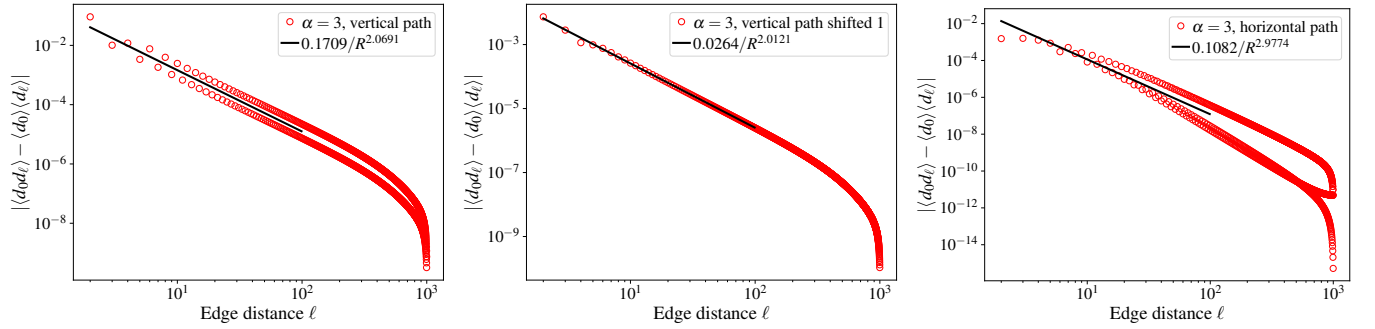

FIG. 11. Dimer-dimer correlator decay on different paths for the triangular lattice on a size 1001×1001 grid with $\alpha = 3$. All plots use a log-log scale. The best fit curves a_1/R^{a_2} are calculated over distances up to 100. For the vertical paths, the decay is power law $\approx C_2/R^2$. For the horizontal path, there appear to be different rates of decay (faster decay than $1/R^2$ but still power-law) depending on the path index.

The vison correlator $|\langle v_0 v_\ell \rangle|$ also decays as a power-law at criticality (Fig. 12), though determining the critical exponent η in the decay is difficult with only finite-size numerics. It is however plausible that one could have $\eta = 1/4$ in agreement with the 2D Ising critical exponent, but we note the numerical values can vary depending on the region used for the linear regression. We
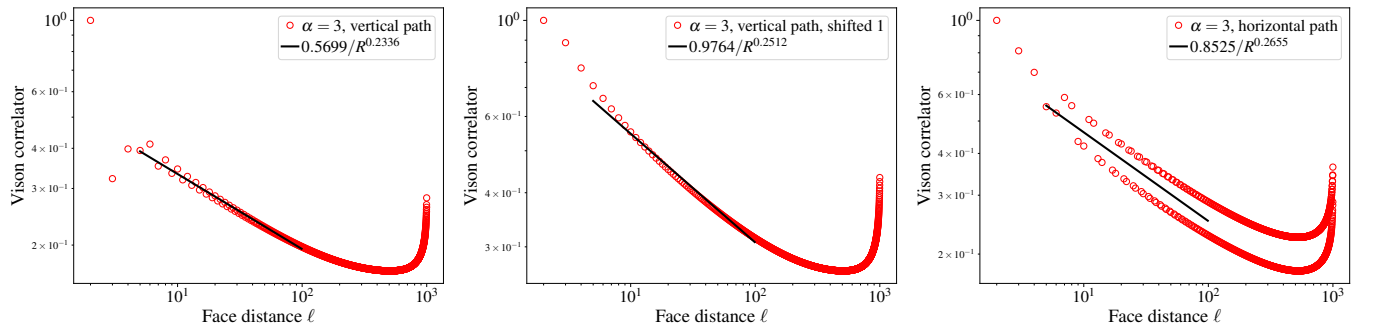

FIG. 12. Vison correlator decay at the critical value $\alpha = 3$ for the triangular lattice on a size 1001×1001 grid. All plots use a log-log scale. The exponent η in the best-fit curve c/R^η is somewhat sensitive to the precise region over which the curve fitting is done (here we use 5 to 100), but a value of $\eta = 1/4$ is plausible.

anticipate that η can be determined more reliably using the infinite-size limit integrals in e.g. Eq. (28).

<h3 style="text-align:center">Double-dimer coverings and constant visons</h3>

In this section we discuss how a phase with only small loops in the double-dimer covering is related to constant vison correlator.

Let $Z = \sum_C \mathcal{W}(C)$ be the classical partition function, where the sum is over all dimer coverings C and $\mathcal{W}(C)$ is the classical weight assigned to the covering. Recall the vison correlator between two faces f_0, f_1 is

$$\langle f_0 f_1 \rangle = \langle (-1)^{\# \text{ dimers along } \gamma} \rangle = \frac{\sum_C (-1)^{\# \text{ dimers along } \gamma} \mathcal{W}(C)}{Z}, \tag{37}$$

where γ is a path between f_0 and f_1. We will consider double-dimer coverings $C \cup C'$, which consist of the edges of two independent random dimer coverings C and C'. We can write the vison correlator squared as

$$|\langle f_0 f_1 \rangle|^2 = \frac{\sum_{C,C'} (-1)^{\# \text{ dimers in } C \cup C' \text{ along } \gamma} \mathcal{W}(C)\mathcal{W}(C')}{Z^2}$$
$$= \mathbb{E}_{C,C'}[(-1)^{\# \text{ dimers in } C \cup C' \text{ along } \gamma}]. \tag{38}$$

Recalling the edges in $C \cup C'$ form only closed loops and double edges, the parity of $\#\{\text{dimers in } C \cup C' \text{ along } \gamma\}$ is unchanged if the path γ enters and exits such a loop or crosses a double edge. So the parity is only affected by loops which contain exactly one of the faces f_0, f_1. For a face f, let $L(f) = \#\{\text{loops in } C \cup C' \text{ that go around } f\}$. Then

$$|\langle f_0 f_1 \rangle|^2 = 2\mathbb{P}_{C,C'}[\#\{\text{dimers in } C \cup C' \text{ along } \gamma\} \text{ is even}] - 1$$
$$= 2\mathbb{P}_{C,C'}[L(f_0) \text{ and } L(f_1) \text{ have the same parity}] - 1. \tag{39}$$

If the loops in $C \cup C'$ are all small, such as seen in the ordered phase in the right-mode part of Fig. 1, then this suggests that $L(f)$ should be a local quantity since it only involves nearby dimers in the small loops. Then $L(f_0)$ and $L(f_1)$ should be nearly independent for far apart faces due to exponential decay of dimer correlations, giving

$$|\langle f_0 f_1 \rangle|^2 = 2(\mathbb{P}[L(f_0), L(f_1) \in 2\mathbb{N}] + \mathbb{P}[L(f_0), L(f_1) \notin 2\mathbb{N}]) - 1$$
$$\approx 2\mathbb{P}[L(f_0) \in 2\mathbb{N}]\mathbb{P}[L(f_1) \in 2\mathbb{N}] + 2\mathbb{P}[L(f_0) \notin 2\mathbb{N}]\mathbb{P}[L(f_1) \notin 2\mathbb{N}] - 1 + O(e^{-cn}). \tag{40}$$

Letting $p_0 = \mathbb{P}[L(f_0) \in 2\mathbb{N}]$ and $p_1 = \mathbb{P}[L(f_1) \in 2\mathbb{N}]$, this becomes

$$|\langle f_0 f_1 \rangle|^2 \approx 2(p_0 p_1 + (1 - p_0)(1 - p_1)) - 1 + O(e^{-cn})$$
$$= 4p_0 p_1 - 2p_0 - 2p_1 + 1 + O(e^{-cn}). \tag{41}$$

To have this tend to 0 as the distance between the faces goes to ∞, we need $p_0 = 1/2$ or $p_1 = 1/2$. If we want the vison correlator to to go to 0 for all paths, then by using periodicity to consider f_0 and f_1 the same type of face, we must have $p := \mathbb{P}[L(f) \in 2\mathbb{N}] = 1/2$ for all faces f (in the infinite size limit). Due to gauge equivalence of edge weights [74, 75], non-uniform edge weights is equivalent to non-uniform face weights. If we have different face weights, or even different face shapes for more complicated lattices, it seems unlikely that we could have all faces have the exact same probability $p_0 = 1/2$. For example, with varying face weights, some faces are likely to have a different average number of edges around them than other faces. Additionally, the condition $p_0 = p_1 = 1/2$ seems very unstable to perturbations. Overall, the above suggests that we will not have a topological spin liquid phase or vison decay if the double-dimer coverings have only small loops.

We conjecture, due to the square-octagon example [57] and related general double-dimer properties of bipartite lattices [35], that it may then be the case that periodic bipartite lattices cannot host a $\mathbb{Z}_2$ quantum spin liquid phase. We emphasize this is a different suggested reasoning than the conventional argument for lack of spin liquid at the RK point on bipartite lattices [2, 48, 49], which argues that such (unweighted) models should be critical. However, this cannot hold for bipartite lattices in general, as the unweighted square-octagon lattice is bipartite but exhibits exponential decay of dimer-dimer correlators.